Effect of Particle Size on Hydrogen Release from Sodium Alanate Nanoparticles

Tim Mueller and Gerbrand Ceder*

Massachusetts Institute of Technology, 77 Massachusetts Avenue 13-5056, Cambridge, Massachusetts 02139

ABSTRACT Density functional theory and the cluster expansion method are used to model 2−10 nm sodium alanate ($NaAlH_4$) nanoparticles and related decomposition products Na_3AlH_6, NaH, and Al. While bulk sodium alanate releases hydrogen in a two-step process, our calculations predict that below a certain size sodium alanate nanoparticles decompose in a single step directly to NaH, Al, and H_2 due to the effect of particle size on decomposition thermodynamics. This may explain why sodium alanate nanoparticles, unlike bulk sodium alanate, have been observed to release hydrogen in the operating temperature range of proton exchange membrane fuel cells. In addition, we identify low-energy surfaces that may be important for the dynamics of hydrogen storage and release from sodium alanate nanoparticles.

KEYWORDS: sodium alanate · $NaAlH_4$ · Na_3AlH_6 · sodium hydride · NaH · aluminum · Al · hydrogen storage · cluster expansion · nanoparticle · density functional theory · surface energy · fuel cell

One of the most difficult remaining technological challenges for hydrogen fuel cells is the storage of hydrogen. Hydrogen storage in solid-state materials has been widely investigated, but it has proven difficult to find a material that stores and releases hydrogen in the rather narrow target temperature range (−40 to 85 °C)[1] for automotive fuel cells. Materials that thermodynamically release hydrogen in this temperature range often suffer kinetic limitations that necessitate higher temperatures. One such material, sodium alanate ($NaAlH_4$), reversibly stores 5.6% hydrogen by weight in a two-step reaction:

$$NaAlH_4 \leftrightarrow (1/3)Na_3AlH_6 + (2/3)Al + H_2 \quad (1)$$

$$Na_3AlH_6 \leftrightarrow 3NaH + Al + (3/2)H_2 \quad (2)$$

At 1 atm, the equilibrium temperatures for reactions 1 and 2 are estimated to be 29 and 109 °C, respectively,[2] but reaction rates at these temperatures are very low. With the addition of catalysts, sufficiently high reaction rates can be achieved at temperatures between 100 and 200 °C but not below 85 °C.[3−5] Recently, it has been reported that 2−10 nm nanoparticles of sodium alanate release hydrogen at temperatures near 70 °C with a significantly lower activation barrier than bulk materials.[6] Subsequent studies have reported similar results, including the observation that for sodium alanate nanoparticles in nanoconfined carbon the two-step decomposition pathway disappears.[7,8] These studies indicate that the use of nanoscale materials might have significant kinetic benefits for hydrogen storage materials, but the reasons for the improved rate of hydrogen release are unknown.

To better understand hydrogen release from sodium alanate nanoparticles, we have used density functional theory[9] (DFT) calculations along with the cluster expansion method[10−14] to predict the shape and energy of $NaAlH_4$, Na_3AlH_6, NaH, and Al nanoparticles. Our calculations indicate that a one-step reaction is thermodynamically favored for the decomposition of small sodium alanate nanoparticles:

$$(NaAlH_4)_n \leftrightarrow (NaH)_n + (Al)_n + (3n/2)H_2 \quad (3)$$

where n is the number of formula units in a nanoparticle. This result, consistent with what is observed experimentally, is primarily a size effect that may be aided by interaction with a supporting material. It is known that nanoparticles may react at different rates than bulk materials due to the short distances over which mass is transported. However our calculations suggest that for sodium alanate the dramatic improvement in reaction kinetics may be due to the fact that an entirely different reaction

*Address correspondence to gceder@mit.edu.

Received for review May 31, 2010 and accepted September 08, 2010.

Published online September 17, 2010.
10.1021/nn101224j

pathway becomes thermodynamically favorable as a function of nanoparticle size.

COMPUTATIONAL APPROACH

Determining the energy of 2−10 nm nanoparticles is computationally challenging. Density functional theory can provide an accurate measure of relative energies between similar systems,[15,16] but it is prohibitively expensive to run density functional theory calculations on nanoparticles more than a few nanometers in diameter. A common approach for estimating particle energies and shapes is the Wulff construction,[17] in which surface energies are calculated for low-energy bulk surfaces, and these energies are used to predict a universal particle shape that is independent of particle size. This method has been used previously for hydride nanoparticles.[18,19] The particle shapes predicted by the Wulff construction will only contain facets for which bulk surface energies are available, whether by experiment or calculation. In addition, the Wulff construction, based on macroscopic surface energies, may not be a valid approximation for facets that are few atoms wide, and particle shape may not be independent of size for particles that are only a few nanometers in diameter.[20,21] This is especially likely if the periodicity of the surface is longer than the facet is wide.

We have employed the cluster expansion method as an alternative to the Wulff construction. The cluster expansion is a lattice model Hamiltonian that has been widely used to study atomic ordering in bulk materials[22−30] and to determine equilibrium crystal shapes for FCC metals.[31] Whereas the Wulff construction applies a macroscopic energy model to small particles, we train a cluster expansion Hamiltonian on small particles and use it to predict the energies of particles of any shape and size. Simulated annealing is then used to find the ground-state shape. As in the Wulff construction, we assume that the structure of the nanoparticle resembles the bulk structure truncated at the surface. The particle may then be thought to sit on a fixed lattice of occupied and unoccupied sites, with the unoccupied sites corresponding to vacuum and the occupied sites corresponding to the particle (Figure 1). We (and others) have observed that there is a very high energy penalty for breaking Al−H bonds,[18] so we constrain the system to ensure that AlH_x complexes remain intact. We assign a "spin variable" value of +1 for occupied sites and −1 for unoccupied sites. The energy of the particle may then be expanded as linear combination "cluster functions", each of which represents the product of the spin variables in a cluster of sites:

$$E(\vec{s}) = \sum_{\text{clusters}} \left(V_{\text{cluster}} \prod_{i \in \text{cluster}} s_i \right) \qquad (4)$$

where $\vec{s}$ is the set of all spin variables, completely describing the shape of the particle, and V_{cluster} are unknown expansion coefficients known as effective cluster interactions (ECI). In practice, symmetry reduces the number of distinct ECI, and all but a finite number of ECI are close to zero. Taking these two insights into account, it is possible to truncate the expansion to a finite number of unknown parameters with little loss of accuracy. The resulting cluster expansion rapidly calculates the energy of a given particle as a sum of contributions from small, localized clusters of sites.

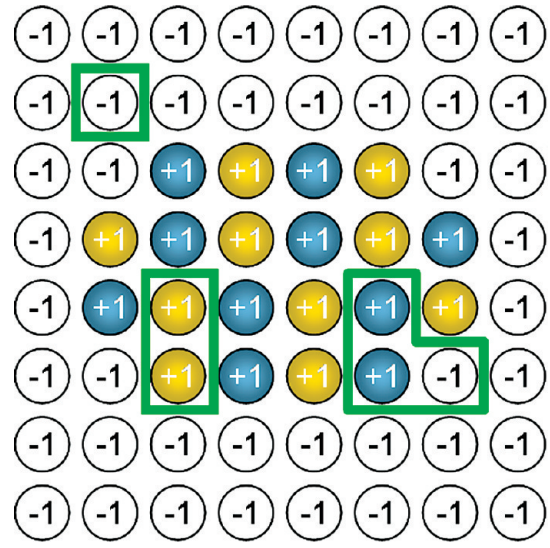

Figure 1. Schematic representation of a cluster expansion for a $NaAlH_4$ nanoparticle. Yellow sites are occupied by Na, blue sites are occupied by AlH_4, and white sites are occupied by vacuum. The spin variables of the Na- and AlH_4-occupied sites have values of +1, and the variables for the unoccupied sites have values of −1. Three sample clusters are outlined in green, representing a cluster of a single site, a nearest-neighbor pair of sites, and a triplet of sites.

The ECI were determined by fitting to a training set of DFT-calculated energies for fully relaxed nanoparticles with diameters between approximately 1 and 3 nm. Because the cluster expansion was trained on relaxed particles, it predicts the energies of relaxed particles including simple surface reconstructions. We did not consider smaller particles in our training set because the relative errors in density functional theory can be significant for such systems.[32] All calculations on $NaAlH_4$, Na_3AlH_6, and NaH were performed on charge-balanced systems, assuming the atoms had oxidation states of Na^{1+}, Al^{3+}, and H^{1-}. The quality of the cluster expansions were evaluated using leave-one-out cross-validation (LOOCV),[13] which provides an estimate of the cluster expansion prediction error.[14] We have used a Bayesian fitting process, which allows for an arbitrarily large number of clusters to be included for a given training set size and has recently been shown to produce cluster expansions with low prediction error.[14]

It was not immediately clear whether aluminum nanoparticles should be based on the bulk FCC lattice or whether they would adopt an icosahedral shape in an attempt to minimize surface energy. It is expected that the smaller the nanoparticle, the more likely a low-

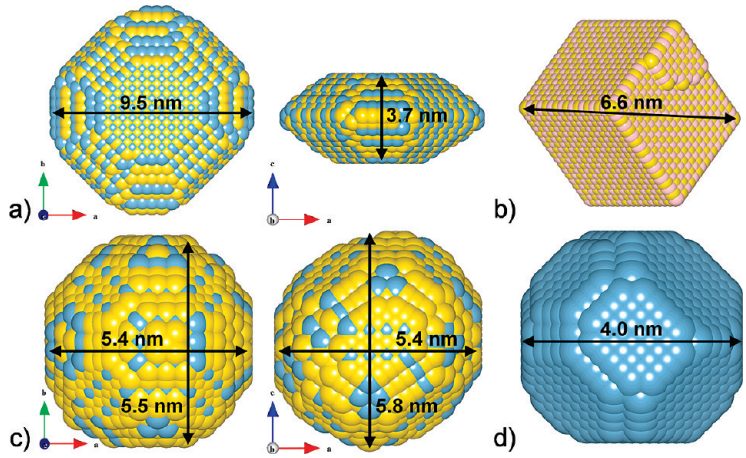

Figure 2. Predicted ground-state shapes for (a) a 15 000 atom $NaAlH_4$ nanoparticle, (b) a 5000 atom NaH nanoparticle, (c) a 9000 atom Na_3AlH_6 nanoparticle, (d) a 2500 atom Al nanoparticle. Orange represents Na, blue represents Al or AlH_x, and in the NaH nanoparticle, pink represents H. The 15 000 atom $NaAlH_4$ nanoparticle has a maximum diameter of nearly 10 nm, and the remaining nanoparticles are approximately the sizes of its decomposition products.

surface energy icosahedral shape is stable. Aluminum nanoparticles with 55 atoms are particularly likely to have an icosahedral structure because 55 atoms can form a perfect icosahedron. However, density functional theory calculations on 55 atom icosahedral and FCC-based aluminum nanoparticles revealed that the FCC-based nanoparticle was more stable by about 6.7 kJ/mol. Because it is unlikely for the icosahedral shape to be relatively more stable for larger nanoparticles or incomplete icosahedra, we modeled aluminum nanoparticles based on an FCC lattice.

RESULTS

Particle Shapes and Surface Energies. We developed cluster expansions for $NaAlH_4$, Na_3AlH_6, NaH, and Al nanoparticles, with LOOCV errors of 0.2, 0.6, 0.6, and 0.6 kJ/mol atoms, respectively. Representative ground-state particle shapes are shown in Figure 2. The predicted $NaAlH_4$ particle shape is flattened along the *c* lattice parameter, and the NaH particle shape is cubic. These are both similar to the shapes previously predicted using Wulff constructions.[18,19] The predicted shapes of the Na_3AlH_6 and Al particles are more isotropic.

The predicted nanoparticle shapes reveal low-energy surfaces for each of these materials. For example, the $NaAlH_4$ nanoparticle shapes predicted by the cluster expansion have prominent {001} surfaces, which are known to have low bulk surface energy.[18,33] The (the Miller indices used in this article are based on the conventional body-centered cubic lattice for $NaAlH_4$ and the primitive monoclinic lattice for Na_3AlH_6). The {116} surface, which was not considered as a potential low-energy surface in previous studies,[18,33] is also prominent on the predicted ground states for $NaAlH_4$ nanoparticles (Figure 3). This low-angle surface may be thought of as short step in the {001} surface (Figure 4) and may be important for the reaction kinetics of $NaAlH_4$. We used density functional theory to calculate the bulk surface energy for prominent $NaAlH_4$ surfaces as well as surfaces previously reported in the literature (Table 1) and found the {116} surface to have the second-lowest known surface energy.

The more isotropic shape of the Na_3AlH_6 particles suggests that a number of different Na_3AlH_6 surfaces are close in surface energy. Supporting this observation, the DFT-calculated surface energies for different bulk Na_3AlH_6 surfaces (Table 1) are close to each other. The calculated Na_3AlH_6 surface energies are significantly higher than the bulk surface energies for $NaAlH_4$, suggesting that these particles are less stable relative to the bulk than the $NaAlH_4$ particles. Significant surface relaxation was observed for some of the Na_3AlH_6

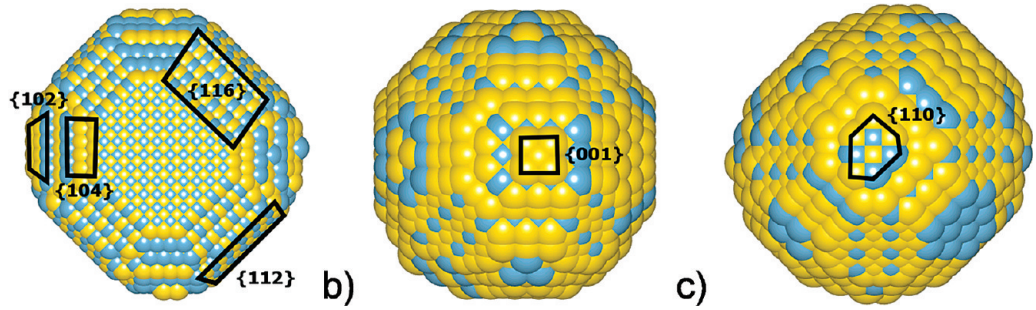

Figure 3. Various surfaces mentioned in the text in the context of predicted nanoparticle shapes: (a) {102}, {104}, {112}, and {116} surfaces of a 15 000 atom $NaAlH_4$ nanoparticle; (b,c) Tasker type 3 {001} and {110} surfaces, respectively, of a 9000 atom Na_3AlH_6 nanoparticle. Orange spheres are sodium, blue spheres are aluminum, and in NaH, light pink spheres are hydrogen.

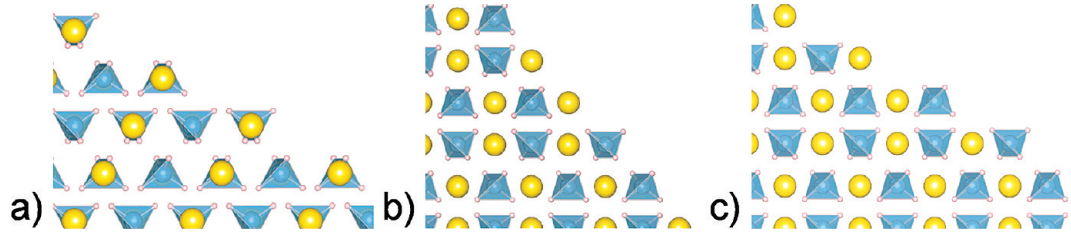

Figure 4. Side views of the (a) {116}, (b) {102}, and (c) {104} surfaces of $NaAlH_4$. Orange spheres are Na, and blue tetrahedra are AlH_4.

particles in the training set, in which some surface Na atoms relaxed several angstroms from their initial positions (Figure 5). It is possible that more complex surface reconstructions exist which have somewhat lower energy than these simple surface relaxations.

The difference between the DFT-calculated surface energies and the cluster-expansion-predicted surface energies are generally small, which is notable considering that the cluster expansion was trained on finite systems. The energy difference generally falls within the variation of surface energies calculated using different implementations of DFT.[33] Unusually large differences are observed for the {102} and {104} $NaAlH_4$ surface energies. These are neutral, long-period surfaces with a pattern of two $(AlH_4)^{1-}$ anions followed by two Na^{1+} cations (Figure 4). The structure of the {102} surface repeats with a period of 1.5 nm, and the {104} surface repeats with a period of 2.3 nm, suggesting that the properties of these surfaces may be different in bulk than in the small nanoparticles used to train the cluster expansion. Due to edge and vertex effects, it might be more energetically favorable to form these surfaces in small particles than in bulk, in which case it should be expected that these surfaces occupy a decreasing fraction of the particle surface area as particle size increases.

In an infinite crystal, certain types of charged surfaces that yield a dipole moment perpendicular to the surface have infinite surface energy per unit area. These surfaces were labeled "type 3" by Tasker, in contrast to "type 1" or "type 2" surfaces for which there is no perpendicular dipole moment.[34] Type 3 surfaces may reduce their surface energies through reconstruction, but the relaxed surface energies are often high for infinite slabs. (For slab calculations, these surface energies may be better described as "cleavage energies" because the slab consists of two different surfaces with opposite charge.) Thermodynamically, it is very unlikely for such surfaces to exist in large crystallites unless there is significant reconstruction. Certain terminations of the {101} surface in $NaAlH_4$, the {111} surface in NaH, and the {110} and {001} surfaces in Na_3AlH_6 are type 3 surfaces. The latter two type 3 surfaces appear on ground-state particle shapes predicted by the cluster expansion (Figure 3). The appearance of these surfaces is due

TABLE 1. Calculated Bulk Surface Energies[a]

material	orientation	termination	DFT surface energy (J/m^2)	CE surface energy (J/m^2)	difference (J/m^2)
$NaAlH_4$	{001}	$NaAlH_4$	0.118	0.110	0.008
	{116}	$NaAlH_4$	0.152	0.164	−0.012
	{112}	$NaAlH_4$	0.162	0.175	−0.012
	{114}	$NaAlH_4$	0.167	0.200	−0.033
	{101}	Na	0.175	0.193	−0.018
	{110}	$NaAlH_4$	0.215	0.237	−0.022
	{101}	AlH_4	0.224	0.231	−0.007
	{103}	AlH_4	0.242	0.197	0.044
	{103}	Na	0.245	0.197	0.048
	{104}	$NaAlH_4$	0.268	0.198	0.070
	{100}	$NaAlH_4$	0.322	0.317	0.006
	{102}	$NaAlH_4$	0.325	0.249	0.076
Na_3AlH_6	{100}	Na_3AlH_6	0.423	0.420	0.003
	{112}	Na_3AlH_6	0.428	0.429	−0.001
	{010}	Na_3AlH_6	0.433	0.435	−0.002
	{001}	Na	0.464	0.482	−0.017
	{110}	Na	0.465	0.466	−0.001
NaH	{100}	NaH	0.197	0.195	0.002
	{110}	NaH	0.477	0.530	−0.053
	{111}	H	0.667	0.650	0.017
	{111}	Na	0.686	0.739	−0.053

[a]These bulk surface energies were calculated for infinite slabs of prominent surfaces on the predicted nanoparticle shapes as well as surfaces reported elsewhere in the literature. Energies were calculated by density functional theory (DFT) and the cluster expansion (CE). The "termination" column indicates which ion was on the outermost face of the slab. In situations in which multiple such terminations were possible, the lowest-energy termination is reported.

to the fact that the cluster expansion was trained on small particles and only considers local interactions (within 1 nm). As a result, the cluster expansion significantly under-predicts the cleavage energies of type 3 surfaces for infinite slabs (Table 2). However, this error is unlikely to have a significant effect on the ground-state shapes and energies of large nanoparticles because these shapes and energies will be generally determined by the terminations with the lowest energy for a given orientation. There is little error in the energies for the lowest-energy surface terminations (Table 2). When the cluster expansion predicts a type 3 surface termination, it is likely that an actual particle will contain a surface with the same orientation, similar energy, and a type 1 or 2 surface termination.

Energetics. Nanoparticle decomposition is different from bulk decomposition in that both the composition and the size of the reaction products must be considered. A particle may decompose into smaller particles, or its decomposition products may be added to existing particles. Decomposition into smaller particles will generally require more energy due to the larger total surface area of the reaction products. To evaluate either pathway, it is necessary to know how the energy of the reaction products varies as a function of particle size. We used the cluster expansion to predict the ground-state energies for $NaAlH_4$ nanoparticles with maximum diameter between 2 and 10 nm, as well as nanoparticles of possible decomposition products Na_3AlH_6, NaH, and Al. The predicted energies of the different nanoparticles as a function of particle size are shown in Figure 6. The nanoparticle energies per formula unit, relative to bulk, are described well by the expression

$$E(n) = \frac{A}{\sqrt[3]{n}} \qquad (5)$$

where n is the number of formula units in the particle, and the value of A for $NaAlH_4$, Na_3AlH_6, NaH, and Al is 102.162, 279.294, 74.956, and 189.968 kJ/mol, respectively. The fact that this expression fits the calculated energies well implies that the average surface energy is nearly independent of particle size.

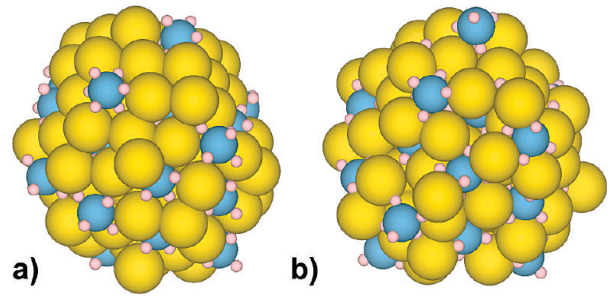

Figure 5. (a) Initial and (b) relaxed atomic positions of a 2 nm Na_3AlH_6 nanoparticle from the cluster expansion training set. Orange spheres are Na, blue spheres are Al, and light pink spheres are H.

We consider three possible reaction paths for $NaAlH_4$ decomposition. We first consider a two-step reaction, similar to the bulk reaction, in which the aluminum released in the second step combines with the aluminum released in the first step to form a single aluminum particle:

$$(NaAlH_4)_n \rightarrow (Na_3AlH_6)_{n/3} + (Al)_{2n/3} + nH_2 \qquad (6)$$

$$(Na_3AlH_6)_n + (Al)_{2n} \rightarrow (NaH)_{3n} + (Al)_{3n} + (3n/2)H_2 \qquad (7)$$

where n indicates the number of formula units per particle. We will refer to eqs 6 and 7 as reactions I and II, respectively. We will also consider a variation of reaction II in which the aluminum released in the decomposition of Na_3AlH_6 forms a separate nanoparticle:

$$(Na_3AlH_6)_n \rightarrow (NaH)_{3n} + (Al)_n + (3n/2)H_2 \qquad (8)$$

We will refer to eq 8 as reaction IIa. Finally, we will consider a one step reaction, which we label reaction III:

$$(NaAlH_4)_n \rightarrow (NaH)_n + (Al)_n + (3n/2)H_2 \qquad (9)$$

The products of reaction III are the same as the reaction products of reaction I followed by reaction II.

Directly calculating these reaction energies can be challenging. Zero-point energy can differ significantly in different hydrogen-containing compounds,[35] and we

TABLE 2. Cleavage Energies for Type 3 Surface Terminations for Bulk Materials[a]

material	orientation	termination	DFT cleavage energy (J/m²)	CE cleavage energy (J/m²)	difference (J/m²)
$NaAlH_4$	{103}	type 3	0.645	0.199	0.445
		lowest energy	0.242	0.197	0.044
	{101}	type 3	1.098	0.325	0.773
		lowest energy	0.175	0.193	−0.018
Na_3AlH_6	{110}	type 3	0.862	0.478	0.384
		lowest energy	0.465	0.466	−0.001
	{001}	type 3	0.986	0.481	0.505
		lowest energy	0.464	0.481	−0.017
NaH	{111}	type 3	1.572	1.106	0.466
		lowest energy	0.667	0.650	0.017

[a]Energies were calculated by density functional theory (DFT) and the cluster expansion (CE). "Type 3" terminations refer to those described by Tasker, and "lowest energy" refers to the lowest-energy surface termination with the given orientation.

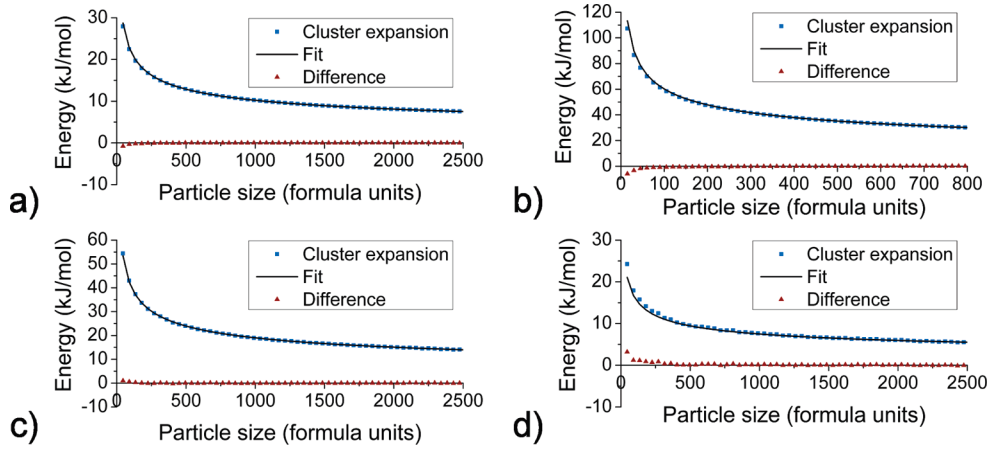

Figure 6. Calculated formation energies (squares) relative to bulk for (a) $NaAlH_4$, (b) Na_3AlH_6, (c) Al, and (d) NaH. The solid lines represent the formation energies fit to eq 5. The *x*-axis is the number of formula units in the particle, and the *y*-axis is the energy relative to the bulk in kJ/mol formula unit.

make no attempt to include zero-point energies in our cluster expansion training sets because it would entail significant computational expense. For similar reasons, we have not modeled the contribution of entropy at finite temperatures. In addition, there are likely to be significant errors in DFT when comparing molecular hydrogen and metallic aluminum to hydrogen and aluminum in ionic compounds, due to the differing chemical environments. To minimize these problems, we calculate the energy of the above reactions relative to the bulk reactions and then add the calculated difference to bulk reaction free energies estimated from experimental data, using parameters given in ref 2. Through this approach, we make the calculated energy of molecular hydrogen irrelevant and aim to maximize the cancellation of errors for the remaining compounds. The resulting Gibbs free energies for reactions I, II, IIa, and III as a function of particle size n and temperature T are given in eqs 10, 11, 12, and 13 respectively.

$$\Delta G_{I}(n,T) = 33.8201 - 0.05654177T - 0.0096014T \ln T + \frac{518.108}{\sqrt[3]{n}} \quad (10)$$

$$\Delta G_{II}(n,T) = 61.4778 + 0.0015413T - 0.0273086T \ln T - \frac{246.384}{\sqrt[3]{n}} \quad (11)$$

$$\Delta G_{IIa}(n,T) = 61.4778 + 0.0015413T - 0.0273086T \ln T - \frac{37.355}{\sqrt[3]{n}} \quad (12)$$

$$\Delta G_{III}(n,T) = 54.3127 - 0.0560280T - 0.0187043T \ln T + \frac{162.762}{\sqrt[3]{n}} \quad (13)$$

where all values are in kJ/mol formula unit. The first three terms on the right side of each expression are from the empirical free energy curves,[2] and the final term is the particle size correction given by eq 5. All of these expressions assume a hydrogen partial pressure of 1 bar.

To compare the calculated results to experimental results, it is necessary to define the relationship between the number of formula units in a $NaAlH_4$ nanoparticle and the experimentally determined nanoparticle size. Here we use the definition that the nanoparticle width d is the cube root of the experimentally determined bulk volume of n formula units:[36]

$$d = \sqrt[3]{0.0716958n} \quad (14)$$

where d is given in nanometers.

Figure 7 shows which reactions are favored as a function of particle size and temperature. As nanoparticles are heated, decomposition will occur *via* either reaction I or reaction III, depending entirely on the nanoparticle size. Reaction I becomes increasingly unfavorable relative to reaction III as nanoparticle size decreases, due to the high surface energy of the Na_3AlH_6 nanoparticles. We predict that reaction I only occurs for $NaAlH_4$ nanoparticles above about 52 nm in diameter. Reaction III is predicted to occur at temperatures as low as approximately 65 °C for nanoparticles 52 nm in diameter. This temperature is comparable to the experimentally observed peak hydrogen desorption temperature for 2−10 nm nanoparticles.[6] Because of the high energy of the decomposition products of 2−10 nm nanoparticles, we predict these particles may start to release hydrogen at 94 °C.

Full decomposition *via* reactions I and II occurs at a lower temperature than full decomposition *via* reactions I and IIa due to differing reaction products. The products of reactions I and II are the same as for reaction III:

$$(NaH)_n + (Al)_n + (3n/2)H_2 \quad (15)$$

and the products of reactions I and IIa are

$$(NaH)_n + (Al)_{2n/3} + (Al)_{n/3} + (3n/2)H_2 \quad (16)$$

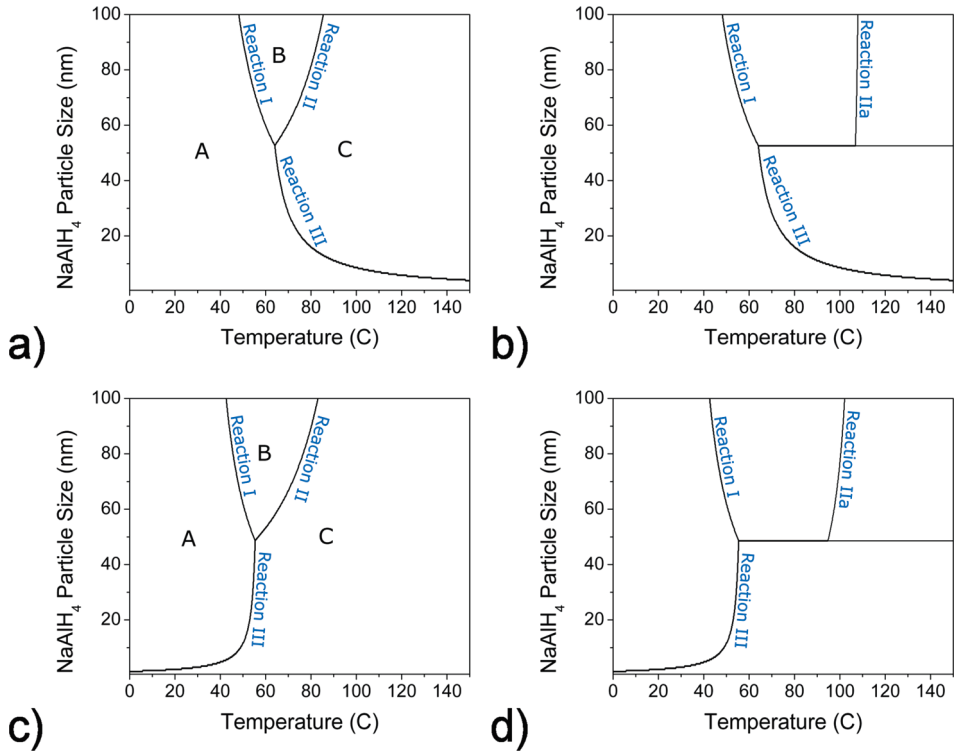

Figure 7. Phase diagrams and reaction maps for sodium alanate nanoparticles as a function of the size of $NaAlH_4$ nanoparticles and temperature. Diagrams (a) and (b) are as calculated, and (c) and (d) are with the formation energy of the NaH and Al decomposition products relative to the bulk reduced by 75%. (a,c) Phase diagrams. In region A, the $NaAlH_4$ particle has the lowest free energy. In region B, the products of the $NaAlH_4$ particle decomposing *via* reaction I have the lowest free energy. In region C, the products of decomposition *via* reaction III, or equivalently reaction I followed by reaction II, have the lowest free energy. (b,d) Reaction maps indicating the thermodynamically favored decomposition reactions as the sodium alanate nanoparticle is heated, under the assumption that the two-step reaction creates two separate aluminum nanoparticles.

Because a single aluminum nanoparticle is created by reactions I and II and two are created by reactions I and IIa, the former two-step reaction occurs at a lower temperature than the latter. If aluminum released in the second step is not deposited on an existing particle, once the original $NaAlH_4$ particle has decomposed *via* reaction I, it is unable to generate the reaction products in eq 15 even though they have lower free energy.

Our calculations provide a possible explanation for the enhanced kinetics of hydrogen desorption from small particles. Below a certain particle size, a one-step reaction becomes favorable at relatively low temperatures due to the effect of nanoparticle size on the thermodynamics of decomposition. Although we have not studied the kinetics of this one-step reaction, it is possible that the activation barrier along the one-step reaction path is lower than the activation barrier along the two-step path, enhancing the rate of both the forward and reverse reactions. It is difficult to specify the exact temperatures and particle sizes at which the one-step reaction becomes favored, but the fact that the formation of Na_3AlH_6 nanoparticles becomes increasingly unfavorable as particle size decreases is supported both by the cluster expansion and by the bulk surface energy calculations. The one-step decomposition reaction is further supported by the fact that Na_3AlH_6 was not reported to be a decomposition product of small $NaAlH_4$ nanoparticles. Despite the approximations made in our calculations, the decomposition path predicted by our calculations corresponds well with the experimental observations.[6−8]

There may be significant surface reconstructions that are not captured by our model, particularly on the high-energy surfaces of Na_3AlH_6 nanoparticles. Because the cluster expansion is trained on relaxed particles, it predicts the energies of particles with simple surface reconstruction (Figure 5). However, lower-energy surface reconstructions that are not simple relaxations may exist, and such reconstructions would make the nanoparticles more stable than our model predicts. If such reconstructions increase the stability of Na_3AlH_6 particles relative to NaH and Al particles, the particle size at which the one-step reaction becomes favored would be reduced.

The conditions in our calculations differ slightly from experimental observations. We assume unsupported nanoparticles, whereas the experiments were conducted on particles supported by carbon. Although our calculations suggest that single-step decomposition for small particles is primarily a thermodynamic size

effect, the support may contribute, especially if it lowers the relative energy of NaH and Al nanoparticles. It is also possible that $NaAlH_4$ does not decompose to smaller particles as we assume. For example, the aluminum produced from $NaAlH_4$ decomposition might be deposited on a large aluminum crystallite, as was observed by Gao *et al.*[7] These pathways could significantly decrease the formation energy for the Al or NaH decomposition products, in which case the temperature at which hydrogen is released *via* the one-step reaction could actually decrease with particle size (Figure 7c,d).

CONCLUSION

We have used the cluster expansion approach to model small nanoparticles of $NaAlH_4$ and possible decomposition products. This approach, trained on small particles, has the advantages that it predicts the energies of small particles well and requires no *a priori* knowledge of low-energy surfaces. The ground-state particle shapes predicted by the cluster expansions contain a variety of facets including surfaces that had not been previously studied.

By combining our calculations with previously reported experimental data, we were able to develop expressions for the energies of nanoparticles as a function of particle size and temperature. These expressions predict that, for small nanoparticles, the bulk two-step reaction for the decomposition of $NaAlH_4$ is replaced by a single-step reaction due to a thermodynamic size effect. This result is consistent with experimental observations, and it may help explain why the decomposition of small nanoparticles is faster than bulk decomposition. The conditions under which the one-step reaction is expected to proceed spontaneously are likely to be influenced by the nanoparticle support and the degree of recombination among decomposition products.

The cluster expansion produces a measure of the average surface energy for the entire nanoparticle, enabling researchers to identify how the relative stability of different compounds evolves as a function of particle size. Although we have applied this approach to the sodium alanate system, it should be widely applicable to the study of the energetics of other small particles. For example, researchers have discovered that relative phase stability is a function of particle size for titania[37] and iron oxide.[38] Using the approach in this paper, it should be possible to calculate size-dependent phase diagrams similar to the ones in Figure 7 for these materials.

It has long been known that reaction kinetics can be influenced by particle size, but this is generally explained in the context of reducing the distances required for mass transport. Our calculations demonstrate that reaction kinetics may also be changed by modifying the thermodynamically favored reaction pathway. This behavior might be seen in other systems in which the particles generated in intermediate steps are expected to have high surface energy.

METHODS

Density functional theory calculations were performed using the Vienna Ab Initio Simulation Package (VASP).[39,40] The PBE GGA exchange-correlation functional[41] and projector-augmented wave (PAW) method[42] were used for all calculations. The standard input files for Al, H, and Na were used, with plane-wave cutoff energies of 240, 250, and 102 eV, respectively. VASP precision was set to high, increasing the plane-wave cutoff energy by 30% for lattice relaxations. For insulators, a *k*-point density of 500 *k*-points per reciprocal atom was used, and for bulk aluminum, a $16 \times 16 \times 16$ *k*-point mesh was used. Nanoparticles were calculated in large supercells with only the *k*-point located at Γ and at least 13 Å spacing between particles. For large insulators such as $NaAlH_4$ nanoparticles, it is best to use Gaussian smearing, and for consistency, this smearing method was used throughout with a width of 0.2 eV for aluminum and 0.05 eV for all other calculations.

Surface energies were calculated on slabs at least 18 Å thick with at least 13 Å vacuum between slabs. For slab calculations, lattice parameters were frozen to the relaxed bulk parameters and all ions were perturbed slightly from their bulk positions to break symmetry and then allowed to relax. Unless otherwise noted, for surfaces in which multiple terminations are possible, the lowest-energy termination that gives symmetric surfaces on either side of the slab was used. For consistency, the same bulk reference energy was used to calculate surface energies and train the cluster expansion. It has been demonstrated that surface energies converge rapidly when the bulk energy is calculated as the derivative of slab energy with respect to slab thickness.[33] This approach was tested for $NaAlH_4$ energies and was found to slightly change the calculated surface energies (by about 0.03 J/m^2) but did not change the order of energies. Bulk energies for $NaAlH_4$ and Na_3AlH_6 were converged so that all forces were less than 1 meV/Å. For all other calculations, the default convergence setting (less than 1 meV difference in total energy between successive ionic steps) was used.

The cluster expansions were trained using Bayesian priors.[14] In all cluster expansions, vacuum was included in the training set, and in all cluster expansions except the icosahedral aluminum expansion, the bulk energy was included in the training set. Linear interpolation between the bulk and vacuum energies was used as the mean for the prior distribution. The widths of the prior distributions were generated using parametrized generating functions, and the parameters of these functions were chosen to minimize the LOOCV error as determined by a conjugate gradient algorithm. It was found that a much better set of generating parameters could be found if both bulk and vacuum were included twice in the training set. This decision had two effects: the LOOCV error becomes essentially an estimate of prediction error for nanoparticles (and not the bulk or surface), and the bulk and vacuum training entries were given double weight in the final fit.

For all cluster expansions, the following generating function was used for the Bayesian prior:

$$\lambda_\alpha = \begin{cases} 0, & \text{if } n_\alpha = 0 \\ \gamma_0, & \text{if } n_\alpha = 1 \\ \gamma_1 e^{\gamma_2 r_\alpha} e^{\gamma_3 n_\alpha}, & \text{if } n_\alpha > 1 \end{cases}$$

where γ_i are positive generating parameters determined by minimizing the LOOCV error, n_α is the number of sites in cluster α, and r_α is the maximum distance between two sites in cluster α. The parameter λ_α is defined in detail in ref 14, and it was found

that this generating function yielded slightly better results than the functions tested in that paper.

Simulated annealing was used to find ground-state shapes. For each system studied, Monte Carlo simulations were run at a temperature high enough to completely disorder the system. The temperature was lowered in steps by a factor of $10^{0.025}$. At each step, the number of Monte Carlo attempts was at least 100 times the number of sites in the total supercell. The annealing was stopped when no fluctuation in energy was observed over two successive steps.

Acknowledgment. This work was funded by the Department of Energy under Grant DE-FG02-05ER46253. Supercomputing resources from the Texas Advanced Computing Center (TACC) are also acknowledged. Crystal structures used in the figures in this text were generated using VESTA.[43]

REFERENCES AND NOTES

1. Hydrogen, Fuel Cells, & Infrastructure Technology Program Multi-Year Research, Development and Demonstration Plan; http://www.eere.energy.gov/hydrogenandfuelcells/mypp/ (accessed December 7, 2009).
2. Lee, B. M.; Jang, J. W.; Shim, J. H.; Cho, Y. W.; Lee, B. J. Thermodynamic Assessment of the NaH <-> Na_3AlH_6 <-> $NaAlH_4$ Hydride System. *J. Alloys Compd.* **2006**, *424*, 370–375.
3. Bogdanovic, B.; Brand, R. A.; Marjanovic, A.; Schwickardi, M.; Tolle, J. Metal-Doped Sodium Aluminium Hydrides as Potential New Hydrogen Storage Materials. *J. Alloys Compd.* **2000**, *302*, 36–58.
4. Sandrock, G.; Gross, K.; Thomas, G. Effect of Ti-Catalyst Content on the Reversible Hydrogen Storage Properties of the Sodium Alanates. *J. Alloys Compd.* **2002**, *339*, 299–308.
5. Jensen, J. O.; Li, Q.; He, R.; Pan, C.; Bjerrum, N. J. 100−200 Degrees C Polymer Fuel Cells for Use with $NaAlH_4$. *J. Alloys Compd.* **2005**, *404*, 653–656.
6. Balde, C. P.; Hereijgers, B. P. C.; Bitter, J. H.; de Jong, K. P. Sodium Alanate Nanoparticles—Linking Size to Hydrogen Storage Properties. *J. Am. Chem. Soc.* **2008**, *130*, 6761–6765.
7. Gao, J. B.; Adelhelm, P.; Verkuijlen, M. H. W.; Rongeat, C.; Herrich, M.; van Bentum, P. J. M.; Gutfleisch, O.; Kentgens, A. P. M.; de Jong, K. P.; de Jongh, P. E. Confinement of NaAlH(4) in Nanoporous Carbon: Impact on H-2 Release, Reversibility, and Thermodynamics. *J. Phys. Chem. C* **2009**, *114*, 4675–4682.
8. Lohstroh, W.; Roth, A.; Hahn, H.; Fichtner, M. Thermodynamic Effects in Nanoscale $NaAlH_4$. *ChemPhysChem* **2010**, *11*, 789–792.
9. Kohn, W.; Sham, L. J. Self-Consistent Equations Including Exchange and Correlation Effects. *Phys. Rev.* **1965**, *140*, A1133–A1138.
10. Sanchez, J. M.; Ducastelle, F.; Gratias, D. Generalized Cluster Description of Multicomponent Systems. *Physica* **1984**, *128A*, 334–350.
11. Blum, V.; Zunger, A. Mixed-Basis Cluster Expansion for Thermodynamics of BCC Alloys. *Phys. Rev. B* **2004**, *70*, 115108.
12. Connolly, J. W. D.; Williams, A. R. Density-Functional Theory Applied to Phase Transformations in Transition-Metal Alloys. *Phys. Rev. B* **1983**, *27*, 5169–5172.
13. van de Walle, A.; Ceder, G. Automating First-Principles Phase Diagram Calculations. *J. Phase Equilib.* **2002**, *23*, 348–359.
14. Mueller, T.; Ceder, G. Bayesian Approach to Cluster Expansions. *Phys. Rev. B* **2009**, *80*, 024103.
15. Wang, Y.; Curtarolo, S.; Jiang, C.; Arroyave, R.; Wang, T.; Ceder, G.; Chen, L. Q.; Liu, Z. K. *Ab Initio* Lattice Stability in Comparison with CALPHAD Lattice Stability. *CALPHAD: Comput. Coupling Phase Diagrams Thermochem.* **2004**, *28*, 79–90.
16. Curtarolo, S.; Morgan, D.; Ceder, G. Accuracy of *Ab Initio* Methods in Predicting the Crystal Structures of Metals: A Review of 80 Binary Alloys. *CALPHAD: Comput. Coupling Phase Diagrams Thermochem.* **2005**, *29*, 163–211.
17. Wulff, G. On the Question of the Rate of Growth and Dissolution of Crystal Surfaces. *Z. Kristallogr.* **1901**, *34*, 449–530.
18. Vegge, T. Equilibrium Structure and Ti-Catalyzed H-2 Desorption in $NaAlH_4$ Nanoparticles from Density Functional Theory. *Phys. Chem. Chem. Phys.* **2006**, *8*, 4853–4861.
19. Kim, K. C.; Dai, B.; Johnson, J. K.; Sholl, D. S. Assessing Nanoparticle Size Effects on Metal Hydride Thermodynamics Using the Wulff Construction. *Nanotechnology* **2009**, *20*, 204001.
20. Marks, L. D. Particle-Size Effects on Wulff Constructions. *Surf. Sci.* **1985**, *150*, 358–366.
21. Marks, L. D. Experimental Studies of Small-Particle Structures. *Rep. Prog. Phys.* **1994**, *57*, 603–649.
22. Ozolins, V.; Wolverton, C.; Zunger, A. Cu−Au, Ag−Au, Cu−Ag, and Ni−Au Intermetallics: First-Principles Study of Temperature-Composition Phase Diagrams and Structures. *Phys. Rev. B* **1998**, *57*, 6427–6443.
23. Sluiter, M. H. F.; Watanabe, Y.; deFontaine, D.; Kawazoe, Y. First-Principles Calculation of the Pressure Dependence of Phase Equilibria in the Al−Li System. *Phys. Rev. B* **1996**, *53*, 6137–6151.
24. Van der Ven, A.; Aydinol, M. K.; Ceder, G.; Kresse, G.; Hafner, J. First Principles Investigation of Phase Stability in Li_xCoO_2. *Phys. Rev. B* **1998**, *58*, 2975–2987.
25. Zarkevich, N. A.; Tan, T. L.; Johnson, D. D. First-Principles Prediction of Phase-Segregating Alloy Phase Diagrams and a Rapid Design Estimate of Their Transition Temperatures. *Phys. Rev. B* **2007**, *75*, 104203.
26. Burton, B. P. Empirical Cluster Expansion Models of Cation Order−Disorder in A(B/sub 1/3/′, B/sub 2/3/″)O/sub 3/ Perovskites. *Phys. Rev. B* **1999**, *59*, 6087–6091.
27. Wolverton, C.; Zunger, A. Prediction of Li Intercalation and Battery Voltages in Layered *vs.* Cubic Li_xCoO_2. *J. Electrochem. Soc.* **1998**, *145*, 2424–31.
28. Seko, A.; Yuge, K.; Oba, F.; Kuwabara, A.; Tanaka, I. Prediction of Ground-State Structures and Order-Disorder Phase Transitions in II−III Spinel Oxides: A Combined Cluster-Expansion Method and First-Principles Study. *Phys. Rev. B* **2006**, *73*, 184117.
29. Kolb, B.; Hart, G. L. W. Nonmetal Ordering in $TiC_{1-x}N_x$: Ground-State Structure and the Effects of Finite Temperature. *Phys. Rev. B* **2005**, *72*, 224207.
30. Garbulsky, G. D.; Ceder, G. Effect of Lattice Vibrations on the Ordering Tendencies in Substitutional Binary Alloys. *Phys. Rev. B* **1994**, *49*, 6327–6330.
31. Wei, S. Q.; Chou, M. Y. First-Principles Determination of Equilibrium Crystal Shapes for Metals at $T = 0$. *Phys. Rev. B* **1994**, *50*, 4859–4862.
32. Wu, Z. G.; Allendorf, M. D.; Grossman, J. C. Quantum Monte Carlo Simulation of Nanoscale MgH_2 Cluster Thermodynamics. *J. Am. Chem. Soc.* **2009**, *131*, 13918–13919.
33. Frankcombe, T. J.; Lovvik, O. M. The Crystal Structure and Surface Energy of $NaAlH_4$: A Comparison of DFT Methodologies. *J. Phys. Chem. B* **2006**, *110*, 622–630.
34. Tasker, P. W. Stability of Ionic-Crystal Surfaces. *J. Phys. C: Solid State Phys.* **1979**, *12*, 4977–4984.
35. Miranda, C. R.; Ceder, G. *Ab Initio* Investigation of Ammonia−Borane Complexes for Hydrogen Storage. *J. Chem. Phys.* **2007**, *126*, 184703.
36. Canton, P.; Fichtner, M.; Frommen, C.; Leon, A. Synchrotron X-ray Studies of Ti-Doped $NaAlH_4$. *J. Phys. Chem. B* **2006**, *110*, 3051–3054.
37. Zhang, H. Z.; Banfield, J. F. Thermodynamic Analysis of Phase Stability of Nanocrystalline Titania. *J. Mater. Chem.* **1998**, *8*, 2073–2076.
38. Navrotsky, A.; Mazeina, L.; Majzlan, J. Size-Driven Structural and Thermodynamic Complexity in Iron Oxides. *Science* **2008**, *319*, 1635–1638.
39. Kresse, G.; Furthmüller, J. Efficiency of *Ab-Initio* Total Energy Calculations for Metals and Semiconductors Using a Plane-Wave Basis Set. *Comput. Mater. Sci.* **1996**, *6*, 15–50.

40. Kresse, G.; Furthmuller, J. Efficient Iterative Schemes for *Ab Initio* Total-Energy Calculations Using a Plane-Wave Basis Set. *Phys. Rev. B* **1996**, *54*, 11169.
41. Perdew, J. P.; Burke, K.; Ernzerhof, M. Generalized Gradient Approximation Made Simple. *Phys. Rev. Lett.* **1996**, *77*, 3865–3868.
42. Blochl, P. E. Projector Augmented-Wave Method. *Phys. Rev. B* **1994**, *50*, 17953–17979.
43. Momma, K.; Izumi, F. VESTA: A Three-Dimensional Visualization System for Electronic and Structural Analysis. *J. Appl. Crystallogr.* **2008**, *41*, 653–658.